CHAPTER 2

Methods and Formalisms

This chapter discusses the origin and development of density functional theory based first-principles method which is the primary tool of investigation employed in this thesis. We begin with the fundamental formulations pertaining to the Kohn-Sham approach which are at the heart of density functional theory and employed in our computations using Quantum ESPRESSO code. We also discuss in brief other methods and codes such as, density functional perturbation theory, ab-initio molecular dynamics simulations (AIMD), ElaStic, BoltzTrap and the ShengBTE code. Followed by methods like, maximally localised wannier functions in Wannier90 and the implementation of tight-binding model in WannierTools code.

2.1 Many-body Problem

The development of quantum theory with theoretical tools such as time-independent Schrödinger equation (presented in Eq. 2.1 where, $\hat{H}$ is the hamiltonian of the system, $\psi(\vec{r})$ is the single particle eigen function and E is the corresponding eigen value), has emerged as an efficient method to describe *simple* quantum systems such as Hydrogen atom.[1] The system of Hydrogen atom is the most simplistic toy model (two-body system with one proton and one electron) wherein the exact solution of Schrödinger equation can be numerically computed by variable separable techniques to obtain the ground state energy of $-$ 13.6 eV. However, as the size of system increases for example, the case of Helium atom, the process of solving the Schrödinger equation gets complicated due to higher number of variables involved

in such many-body systems which makes finding the exact numerical solution a challenging task which can be adderssed by reducing the system to a two-body system with reduced mass.

$$\hat{H}\psi(\vec{r}) = E\psi(\vec{r}) \tag{2.1}$$

However, the complexity scales-up exponentially as we consider the periodic arrangement of atoms in solids which are regarded as many-electron systems with indistinguishable mutual interactions in a smeared-out background positive nuclear charge. Such a system is described by the 'N' particle eigen function $\psi(\vec{r}_1, \vec{r}_2, \vec{r}_3, ..., \vec{r}_N)$.[2] It is next to impossible; to find the exact solution (as in the case of Hydrogen atom) of such a complex many-body system. To add to this, in such big systems, we also come across complex interactions between electron-electron, electron-ion and ion-ion making the Hamiltonian of the system quite complex as presented in Eq. 2.2. Here, $\hat{T}_e$, $\hat{T}_n$, $\hat{V}_{e,e}$, $\hat{V}_{e,n}$ and $\hat{V}_{n,n}$ are, the kinetic and potential energy operators (accuonting for electron-electron, electron-ion and ion-ion interactions) respectively.[3,4]

$$\hat{H} = \hat{T}_e + \hat{T}_n + \hat{V}_{e,e} + \hat{V}_{e,n} + \hat{V}_{n,n} \tag{2.2}$$

Then, the many-body time-independent version of Shcrödinger equation reduces to Eq. 2.3 where, the indices i and k run over the electrons and ions, m_e and m_n are mass of electrons and ions, Z_k and $\mathrm{Z}_{k'}$ are the nuclear charge on ions, $|\vec{r}_{n,k} - \vec{r}_{n,k'}|$, $|\vec{r}_i - \vec{r}_j|$ and $|\vec{r}_i - \vec{r}_{n,k}|$ are the radial distances between ion-ion, electron-electron and electron-ion respectively.

$$\hat{H}\psi(\vec{r}) = \Bigg(-\frac{\hbar^2}{2m_e}\sum_i \frac{\partial^2}{\partial \vec{r}_i^2} - \frac{\hbar^2}{2m_n}\sum_k \frac{\partial^2}{\partial \vec{r}_{n,k}^2} + \frac{1}{2}\sum_{\substack{k,k' \\ k\neq k'}} \frac{e^2}{4\pi\epsilon_0}\frac{Z_k Z_{k'}}{|\vec{r}_{n,k} - \vec{r}_{n,k'}|} + \frac{1}{2}\sum_{\substack{i,j \\ i\neq j}} \frac{e^2}{4\pi\epsilon_0}\frac{1}{|\vec{r}_i - \vec{r}_j|} - \sum_i \sum_k \frac{e^2}{4\pi\epsilon_0}\frac{Z_k}{|\vec{r}_i - \vec{r}_{n,k}|} \Bigg)\psi(\vec{r}) = E\psi(\vec{r}) \tag{2.3}$$

Solving Eq. 2.3 gives the information regarding the ground state of the system in terms of the energy eigen values and since this equation depends on the atomic mass and charge of the electrons and ions, the method is termed as *first-principles* as it does not require parametric fitting to obtain the solution as in the case of empirical problem. However, the associated complexities persist making it impossible to solve Eq. 2.3 for a many body system. An attempt by Born and Oppenheimer was made to address this issue and make the equation solvable.

2.2 Eigen Function Based Approximations

Born-Oppenheimer Approach

As an analogy, imagine you are driving down a four-lane highway in a car, you can travel faster and overtake several heavy vehicles such as trucks, rollers etc. So, when we want to study the speed of vehicles travelling in such a scenario, we can neglect the effect of slow moving heavy vehicles. Similarly, when the electrons and ions are confined in a momentum space, by the virtue of mass, the electrons would posses higher momentum as compared to the ions. Hence, we can neglect the ionic contribution in the Hamiltonian presented in Eq. 2.2, this is known as the Born-Oppenheimer approximation.[5] Based on this, the electrons are assumed to move in a smeared-out background positive charge originating from the relatively static ions. Then, the eigen functions can be presented as a combination of the electronic and ionic eigen functions as evident from Eq. 2.4 where, $\chi_k(\vec{r}_n)$ and $\phi_i(\vec{r}_i, \vec{r}_n)$ are the ionic and electronic eigen functions respectively.

$$\psi(\vec{r}) = \chi_k(\vec{r}_n)\phi_i(\vec{r}_i, \vec{r}_n) \tag{2.4}$$

Then, the variable separated form of Eq. 2.3 can be presented as Eq. 2.5 and Eq. 2.6 below.

$$\left(-\frac{\hbar^2}{2m_n}\sum_k \frac{\partial^2}{\partial \vec{r}_{n,k}^2} + \frac{1}{2}\sum_{\substack{k,k' \\ k\neq k'}} \frac{e^2}{4\pi\epsilon_0}\frac{Z_k Z_{k'}}{|\vec{r}_{n,k} - \vec{r}_{n,k'}|} \right)\chi_k(\vec{r}_n) = E\chi_k(\vec{r}_n) \tag{2.5}$$

$$\left(-\frac{\hbar^2}{2m_e}\sum_i \frac{\partial^2}{\partial \vec{r}_i^2} + \frac{1}{2}\sum_{\substack{i,j \\ i\neq j}} \frac{e^2}{4\pi\epsilon_0}\frac{1}{|\vec{r}_i - \vec{r}_j|} - \sum_i\sum_k \frac{e^2}{4\pi\epsilon_0}\frac{Z_k}{|\vec{r}_i - \vec{r}_{n,k}|} \right)\phi_i(\vec{r}_i, \vec{r}_n) = E\phi(\vec{r}_i, \vec{r}_n) \tag{2.6}$$

Under the Born-Oppenheimer approximation, the first term of Eq. 2.5 vanishes resulting in a constant (β).[6] Then the modified Hamiltonian can be rewritten as in Eq. 2.7 where, $\hat{T}_e = -\frac{\hbar^2}{2m_e}\sum_i \frac{\partial^2}{\partial \vec{r}_i^2}$ is the electron kinetic energy operator, $\hat{V}_{e,e} = \frac{1}{2}\sum_{\substack{i,j \\ i\neq j}} \frac{e^2}{4\pi\epsilon_0}\frac{1}{|\vec{r}_i - \vec{r}_j|}$ is the electron-electron interaction potential, $\hat{V}_{e,n} = -\sum_i\sum_k \frac{e^2}{4\pi\epsilon_0}\frac{Z_k}{|\vec{r}_i - \vec{r}_{n,k}|}$ is the electron-ion interaction potential and $\beta = \frac{1}{2}\sum_{\substack{k,k' \\ k\neq k'}} \frac{e^2}{4\pi\epsilon_0}\frac{Z_k Z_{k'}}{|\vec{r}_{n,k} - \vec{r}_{n,k'}|}$ is an external potential ($\hat{V}_{ext}$). The reduced form of Schrodinger equation can then be presented as in Eq. 2.8

$$\hat{H} = \hat{T}_e + \hat{V}_{e,e} + \hat{V}_{e,n} + \beta \tag{2.7}$$

$$\hat{H}\phi(\vec{r}) = \left(-\frac{\hbar^2}{2m_e}\sum_i \frac{\partial^2}{\partial \vec{r}_i^2} + \frac{1}{2}\sum_{\substack{i,j \\ i\neq j}} \frac{e^2}{4\pi\epsilon_0}\frac{1}{|\vec{r}_i - \vec{r}_j|} + \hat{V}_{e,n} + \hat{V}_{ext} \right)\phi(\vec{r}) = E\phi(\vec{r}) \tag{2.8}$$

This approximation partly solves the complexity of many-body Schrödinger equation since, it does not address the electron-electron interactions and the assymetry and correlations which govern Fermions like electrons. This was addressed by the, Hartree and Hartree-Fock approximations.

Hartree Approach

The coulomb interactions between electrons governed by classical electrostatics had to be addressed in order to further simplify the many-body problem. This was done by Hartree who, modified the many-body problem to one-electron problem which is known as the independent electron approximation.[7–10] The electron-electron interaction potential (independent of the self-interactions) contributing to the Hamiltonian presented in Eq. 2.7 can be written in terms of the charge density ρ(r) as in Eq. 2.9.

$$\hat{V}_{e,e}(r) = \int \frac{[\rho(r') - \rho_i(r')]}{|r - r'|} dr' \tag{2.9}$$

According to classical electrostatics, the distribution of electronic charge density in space ρ(r) gives rise to an electrostatic potential V_l(r) which is governed by the Poisson's relation presented in Eq. 2.10. The electrons in such an electrostatic potential would have a potential energy known as the Hartree potential V_H(r) which obeys the Poisson's relation and transforms in Hartree units as, $V_H(r) = -V_l(r)$.

$$\nabla^2 V_l(r) = \frac{\rho(r)}{\epsilon_0} \tag{2.10}$$

Then, the electronic charge distribution corresponding to the Hartree potential can be constructed by summing the individual eigen states as below with the summation running over all the occupied eigen states;

$$\rho(r) = \sum_m |\psi_m(r)|^2 \tag{2.11}$$

With this, the electron-electron interaction potential gets converted to a single electron potential as presented in Eq. 2.13 (by using Eq. 2.11 in Eq. 2.9) which is also known as the Hartree potential.

$$\hat{V}_{e,e}(r) = V_l(r) = \sum_{m \neq l} \int \frac{|\psi_m(r)|^2}{|r - r'|} dr' \tag{2.12}$$

Hartree also suggested to present many-body eigen function as the product of eigen functions of individual electrons comprising the system as presented in Eq. 2.13 below.

$$\psi(\vec{r}_1, \vec{r}_2, ..., \vec{r}_N) = \prod_{m=1}^{N} \psi(\vec{r}_m) \tag{2.13}$$

Then, by introducing the Hartree potential presented in Eq. 2.12 in Eq. 2.8 we get the modified Schrödinger equation as follows (Eq. 2.14) which is known as the Hartree equation.

$$\left(- \frac{\hbar^2}{2m_e} \sum_i \frac{\partial^2}{\partial \vec{r}_i^2} + \sum_{m \neq l} \int \frac{|\psi_m(r)|^2}{|r - r'|} dr' + \hat{V}_{e,n} + \hat{V}_{ext} \right) \psi(\vec{r}) = E\psi(\vec{r}) \tag{2.14}$$

However, the missing piece was that, Hartree did not include the electronic correlations which led to the Hartree-Fock approximations.[11,12]

Hartree-Fock Approach

The major problem with Hartree approach was that, (i) the eigen functions of electrons were not anti-symmetric with respect to exchange of electrons and, (ii) the electron-electron interactions were averaged. Hartree-Fock method addresses the former problem (which was pointed out by Slater and Fock independently).[13,14]

They began with anti-symmetric eigen function as a function of the position and spin (presented in Eq. 2.15 below) which satisfies the Pauli exclusion principles which mandates that, under particle exchange, the eigen functions would be anti-symmetric. As a consequence, no two electrons can have the same set of quantum numbers i.e., electrons with same spin cannot simultaneously occupy the same eigen state.

$$\psi_{HF}\left[(\vec{r}_1, \sigma_1), (\vec{r}_2, \sigma_2), ..., (\vec{r}_N, \sigma_N)\right] = -\psi_{HF}\left[(\vec{r}_1, \sigma_1), (\vec{r}_2, \sigma_2), ..., (\vec{r}_N, \sigma_N)\right] \tag{2.15}$$

Also, instead of using the product of eigen functions presented in Eq. 2.13, we use a Slater determinant eigen function which satisfies anti-symmetry and is presented in Eq. 2.16 where, $\psi_r(\vec{r}_s, \sigma_s)$ are one electron eigen functions.[15]

$$S = \frac{1}{\sqrt{N!}} \begin{vmatrix} \psi_1(\vec{r}_1, \sigma_1) & \psi_1(\vec{r}_2, \sigma_2) & ... & \psi_1(\vec{r}_N, \sigma_N) \\ \psi_2(\vec{r}_1, \sigma_1) & \psi_2(\vec{r}_2, \sigma_2) & ... & \psi_2(\vec{r}_N, \sigma_N) \\ \vdots & \vdots & ... & \vdots \\ \psi_N(\vec{r}_1, \sigma_1) & \psi_N(\vec{r}_2, \sigma_2) & ... & \psi_N(\vec{r}_N, \sigma_N) \end{vmatrix} \tag{2.16}$$

Then using the Lagrangian multiplier method to minimize the expectation value of the Hamiltonian as done to obtain Eq. 2.14 we arrive at the set of Hartree-Fock equations presented in Eq. 2.17 where, s_m and s_l are spin labels. Although the electron exchange is addressed but this approach is computationally expensive, since, the total energy of the system E in Eq. 2.17 requires minimization of the 'N' particle Slater determinant.

$$\left(-\frac{\hbar^2}{2m_e} \sum_i \frac{\partial^2}{\partial \vec{r}_i^2} + \hat{V}_{e,n} + \hat{V}_{ext} + \sum_{m \neq l} \int \frac{|\psi_m(r)|^2}{|r - r'|} dr' - \sum_m \delta_{s_m, s_l} \int \frac{\psi_m^*(r')\psi_l(r')}{|r - r'|} dr' \right) \psi(\vec{r}) = E\psi(\vec{r}) \tag{2.17}$$

The complexity of many-body Schrödinger equation is that, for a system with 'N' electrons, there would be $3N$ degrees of freedom which increases the number of variable in the problem. Density Functional Theory resolves this issue by apprixomating the many-body problem to a single electronic density which is computationaly viable.

2.3 Density Based Approximations

Thomas-Fermi Approach

Thomas and Fermi proposed that, the total energy of a system can be written as a functional of the electron density rather than considering the single particle eigen functions proposed by Hartree and Hartree-Fock approaches.[16,17] Therefore, the kinetic energy of an 'N' interacting electrons can be expressed in terms of the electron density ($n(\vec{r})$) as in Eq. 2.18. Then the total energy (E) can be expressed as a functional of electron density as in Eq. 2.19 where, the kinetic energy, electrostatic energy and external potential are expressed as a functional of electron density.

$$T_{TF} = C_k \int n(\vec{r})^{5/3} d^3r \tag{2.18}$$

$$E = C_k \int n(\vec{r})^{5/3} d^3r + \int \hat{V}_{ext}(\vec{r}) n(\vec{r}) + \frac{1}{2} \iint \frac{e^2}{4\pi\epsilon_0} \frac{n(\vec{r}')n(\vec{r})}{|r - r'|} d^3r d^3r' \tag{2.19}$$

Then by proceeding with the Lagrangian multiplier method, the above equation can be minimized.[18] However a drawback is that, this approach does not include the electron exchange. Although it was addressed by Dirac by including the exchange interaction and correlation functional but, the shell structure and behaviour of atoms in complex systems could not be established.[19,20]

Hohenberg-Kohn Approach

Hohenberg and Kohn devised two theorems which are at the core of Density Functional Theory.[21] The two theorems are stated below.

Theorem I:

"*The external potential $\hat{V}_{ext}(\vec{r})$, and hence the total energy, is a unique functional of the electron density $n(\vec{r})$.*"

The energy functional as established in the theorem above can be expressed in terms of the external potential as in Eq. 2.20 where, F[n($\vec{r}$)] is an unknown universal functional of the electron density n($\vec{r}$).

$$E[n(\vec{r})] = \int \hat{V}_{ext}(\vec{r}) n(\vec{r}) dr + F[n(\vec{r})] \tag{2.20}$$

$$E[n(\vec{r})] = \langle \psi | \hat{H} | \psi \rangle \tag{2.21}$$

Assuming that a non-degenerate ground state exists, a Hamiltonian (presented in Eq. 2.22) can be designed corresponding to the total energy functional (presented in Eq. 2.20) such that, the eigen function minimizes the expectation value (presented in Eq. 2.21) giving the ground state of the system.

$$\hat{H} = \hat{F} + \hat{V}_{ext} \tag{2.22}$$

$$\hat{F} = \hat{T}_e + \hat{V}_{e,e} \tag{2.23}$$

Where, the electronic Hamiltonian $\hat{F}$ consists the kinetic energy and electron-electron interaction potential as presented in Eq. 2.23. This is identical to every 'N' electron system such that, the Hamiltonian is completely described by 'N' electrons and external potential $\hat{V}_{ext}(\vec{r})$.

Consider two unique external potentials, ${}^1\hat{V}_{ext}(\vec{r})$ and ${}^2\hat{V}_{ext}(\vec{r})$ which would result into identical electron density n($\vec{r}$). Then, the corresponding Hamiltonians ${}^1\hat{H}$ and ${}^2\hat{H}$ would lead to unique ground states ${}^1\psi$ and ${}^2\psi$ respectively such that the corresponding electron density is n($\vec{r}$). Then by applying variational principle and using Eq. 2.23 we get;

$$\begin{aligned} {}^1E_0 < \langle {}^2\psi | {}^1\hat{H} | {}^2\psi \rangle &= \langle {}^2\psi | {}^2\hat{H} | {}^2\psi \rangle + \langle {}^2\Psi | {}^1\hat{H} - {}^2\hat{H} | {}^2\psi \rangle \\ &= {}^2E_0 + \int n(\vec{r})[{}^1\hat{V}_{ext}(\vec{r}) - {}^2\hat{V}_{ext}(\vec{r})]dr \end{aligned} \tag{2.24}$$

$${}^2E_0 < {}^1E_0 + \int n(\vec{r})[{}^1\hat{V}_{ext}(\vec{r}) - {}^2\hat{V}_{ext}(\vec{r})]dr \tag{2.25}$$

$${}^1E_0 + {}^2E_0 < {}^2E_0 + {}^1E_0 \tag{2.26}$$

Where, ${}^1E_0$ and ${}^2E_0$ are the ground state energies corresponding to the Hamiltonians ${}^1\hat{H}$ and ${}^2\hat{H}$ respectively. Adding Eq. 2.24 and Eq. 2.25 we get Eq. 2.26 which contradicts our assumptions and proves that, there can be only one external potential $\hat{V}_{ext}$ which uniquely determines the ground state density n($\vec{r}$) and vice-versa.

Theorem II:

"*The groundstate energy can be obtained variationally: the density that minimises the total energy is the exact groundstate density.*"

The eigen functions of 'N' particle system is governed by the Hamiltonian $\hat{H}$ which is governed by the external potential $\hat{V}_{ext}$ and the number of particles, off which the external potential is governed by the electron density n($\vec{r}$) as evident from Theorem I. This indicates that, the eigen function is a functional of the electron density n($\vec{r}$), this implies that the expectation value of $\hat{F}$ is also a functional of the electron density n($\vec{r}$) as evident from Eq. 2.27.

$$F[n(\vec{r})] = \langle \psi | \hat{F} | \psi \rangle \tag{2.27}$$

Consider an energy functional $E_x[n(\vec{r})]$ (presented in Eq. 2.28) wherein the external potential $\hat{V}_{ext}$ is independent of an unknown electron density $n'(\vec{r})$.

$$E_x[n(\vec{r})] = \int \hat{V}_{ext}(\vec{r}) n'(\vec{r}) dr + F[n'(\vec{r})] \tag{2.28}$$

Then according to the variational principle,

$$\langle \psi' | \hat{F} | \psi' \rangle + \langle \psi' | \hat{V}_{ext}(\vec{r}) | \psi' \rangle > \langle \psi | \hat{F} | \psi \rangle + \langle \psi | \hat{V}_{ext}(\vec{r}) | \psi \rangle \tag{2.29}$$

Where, ψ is the eigen function corresponding to the correct ground state electron density $n(\vec{r})$. This gives us;

$$\int n'(\vec{r}) \hat{V}_{ext}(\vec{r}) dr + F[n'(\vec{r})] > \int n(\vec{r}) \hat{V}_{ext}(\vec{r}) dr + F[n(\vec{r})] \tag{2.30}$$

Then, following the variational principle we arrive at;

$$E_x[n'(\vec{r})] > E_x[n(\vec{r})] \tag{2.31}$$

This implies that, the ground state energy and the corresponding electron density $n(\vec{r})$ is lower than any other electron density $n'(\vec{r})$. The above variational principle is known as the Hohenberg-Kohn theorem wherein, The universal functional $\hat{F}[n(\vec{r})]$ yields the lowest energy state if and only if the input electron density is the true ground state electron density $n(\vec{r})$.

Kohn-Sham Approach

The Kohn-Sham approach established Density Functional Theory as a practical tool to obtain the ground state of a system.[22] In this approach, the electron density $n(\vec{r})$ is parametrized into one electron orbital $\zeta_i(\vec{r})$ (where summation is over all the occupied states) as in Eq. 2.32 with the total energy functional expressed as in Eq. 2.33.

$$n(\vec{r}) = \sum_i \zeta_i^*(\vec{r}) \zeta_i(\vec{r}) \tag{2.32}$$

$$E[n(\vec{r})] = T[n(\vec{r})] + E_H[n(\vec{r})] + E_{xc}[n(\vec{r})] + E_{ext}[n(\vec{r})] \tag{2.33}$$

Here, E_H is the electron-electron interaction under Hartree approximation, E_{ext} is the external potential and the kinetic energy of the non-interacting electrons in $\zeta_i(\vec{r})$ are given as follows;

$$E_H[n(\vec{r})] = \iint \frac{n(\vec{r})n(\vec{r'})}{|\vec{r} - \vec{r'}|} dr dr' \tag{2.34}$$

$$E_{ext}[n(\vec{r})] = \int \hat{V}_{ext} n(\vec{r}) dr \tag{2.35}$$

$$T[n(\vec{r})] = \sum_i \int \zeta_i^*(\vec{r}) \big(-\frac{1}{2}\nabla^2 \big) \zeta_i(\vec{r}) d^3r \tag{2.36}$$

The remaing quantity in Eq. 2.33 is known as the exchange-correlation energy $E_{xc}[n(\vec{r})]$. As the single electron orbitals $\zeta_i(\vec{r})$ are variational quantities, the variation of the total energy functional with respect to these orbitals $\zeta_i^*(\vec{r})$ would result into an effective single electron equation known as the Kohn-Sham equation, presented in Eq. 2.37 below.

$$\left(-\frac{1}{2}\nabla^2 + \int \frac{n(\vec{r'})}{|\vec{r} - \vec{r'}|} dr' + \hat{V}_{ext}[n(\vec{r})] + \frac{\delta E_{xc}[n(\vec{r})]}{\delta n(\vec{r})} \right) \zeta_i(\vec{r}) = \epsilon_i \zeta_i(\vec{r}) \tag{2.37}$$

The Kohn-Sham equation for electrons in a potential are given by Eq. 2.38 where, the exchange-correlation potential is obtained by the variation of exchange-correlation energy as presented in Eq. 2.39.

$$V_{eff}(\vec{r}) = V_{ext}(\vec{r}) + \int \frac{n(\vec{r'})}{|\vec{r} - \vec{r'}|} d^3r' + V_{xc}[n(\vec{r})] \tag{2.38}$$

$$V_{xc}[n(\vec{r})] = \frac{\delta E_{xc}[n(\vec{r})]}{\delta n(\vec{r})} \tag{2.39}$$

Therefore, the modified form of the Kohn-Sham equation is as follows;

$$\left(-\frac{1}{2}\nabla^2 + V_{eff}(\vec{r}) \right) \zeta_i(\vec{r}) = \epsilon_i \zeta_i(\vec{r}) \tag{2.40}$$

Here, ϵ_i are the Lagrange parameters introduced to retain the orthogonality of the single-particle Kohn-Sham orbitals as follows;

$$\int \zeta_i^*(\vec{r}) \zeta_j(\vec{r}) d^3r = \delta_{ij} \tag{2.41}$$

2.4 Exchange and Correlation Functionals

The exchange and correlation functionals in Kohn-Sham approach define the accuracy of calculations and outcomes. Since the theory was established, several functionals have been developed with a goal to perdict chemically accurate results. Broadly, they can be classified and understood in terms of the Jacob's ladder wherein the computational cost increases as we move up the rungs towards a chemically accurate picture of the system under investigation. The exchange and correlation functionals are required to follow certain constraints i.e., (i) these functionals show be slow varying densities and should reduce to homogenous two dimensional electron gas limit, (ii) they should be asymptotic for atoms/molecules (i.e., $V_{xc}[n(\vec{r})] \rightarrow -\frac{1}{\vec{r}}$ for $\vec{r} \rightarrow \infty$) and (iii) they should not be self-interacting. These functionals can be classified as, local, semi-local and non-local functionals.

Local Density Approximation

Local density approximation and local spin-density approximations are presented in Eq. 2.42 and 2.43 respectively.[21] These are known as local functionals since, the exchange energy functional depends on the electron density and spin at some point $\vec{r}$ in the electron cloud of the atom.

$$E_{xc}^{LDA}[n(\vec{r})] = \int \epsilon_{xc}[n(\vec{r})]n(\vec{r})d^3r \tag{2.42}$$

$$E_{xc}^{LSDA}[n_{\uparrow}(\vec{r}), n_{\downarrow}(\vec{r})] = \int \epsilon_{xc}[n_{\uparrow}(\vec{r}), n_{\downarrow}(\vec{r})]n(\vec{r})d^3r \tag{2.43}$$

Generalized Gradient Approximation

Generalised gradient approximation and generalised spin-gradient apparoximations are presented in Eq. 2.44 and 2.45 respectively.[23,24] These functionals are known as semi-local functionals since, the energy functional depends on the electron density and their gradients at some point $\vec{r}$ and its neighbouthood. One of the well known and most widely used semi-local functional is PBE.

$$E_{xc}^{GGA}[n(\vec{r})] = \int \epsilon_{xc}[n(\vec{r}), \nabla n(\vec{r})]n(\vec{r})d^3r \tag{2.44}$$

$$E_{xc}^{GSGA}[n_{\uparrow}(\vec{r}), n_{\downarrow}(\vec{r})] = \int \epsilon_{xc}[n_{\uparrow}(\vec{r}), n_{\downarrow}(\vec{r}), \nabla n_{\uparrow}(\vec{r}), \nabla n_{\downarrow}(\vec{r})] n(\vec{r}) d^3r \tag{2.45}$$

When the kinetic energy densities (presented in Eq. 2.36) are included, we arrive at another semi-local functional, the meta-generalised gradient approximation (presented generally as in Eq. 2.46).[25,26] In such functionals, apart from the gradients, we also consider the Laplacians of density. Although, these functionals exhibit divergent nature when applied on diatomic systems but, they are useful to identify the type of bond in the system i.e., covalent or metallic. Some of the frequently used functionals are TPSS and SCAN.

$$E_{xc}^{meta-GGA}[n_{\uparrow}(\vec{r}), n_{\downarrow}(\vec{r})] = \int \epsilon_{xc}[n_{\uparrow}(\vec{r}), n_{\downarrow}(\vec{r}), \nabla n_{\uparrow}(\vec{r}), \nabla n_{\downarrow}(\vec{r}), \nabla^2 n_{\uparrow}(\vec{r}), \nabla^2_{\downarrow}(\vec{r})] n(\vec{r}) d^3r \tag{2.46}$$

Hybrid Approximation

Hybrid functionals are a class of non-local functionals which are computationally quite expensive but, preferred over other approximations since they provide chemically acurate results.[27] In such functionals the energy functional depends on the density or orbitals everywhere in the electron cloud of the atom. The advantage of such functionals are; (i) we can get rid of the self-interaction term and (ii) we can get correct asymptotic form i.e., $-\frac{1}{\vec{r}}$ for large $\vec{r}$. The simple solution is to establish a exchange correlation energy funtional as in Eq. 2.47. But, this has mathematical problem of error cancellation in LDA and GGA i.e., the error of exchange in LDA and correlation in LDA cancel eachother with the errors in LDA correlation being quite large as compared to the exact exchange. So the solution is achieved by introducing a mixing parameter ($\alpha; 0 < \alpha < 1$) which modifies Eq. 2.47 into Eq. 2.48 which takes the form of Eq. 2.49 for the PBE0 functional (one of the first hybrid functionals).

$$E_{xc}^{hybrid}[n(\vec{r})] = E_x^{exact}[n(\vec{r})] + E_c^{LDA/GGA}[n(\vec{r})] \tag{2.47}$$

$$E_{xc}^{hybrid}[n(\vec{r})] = \alpha E_x^{exact}[n(\vec{r})] + (1-\alpha) E_x^{GGA}[n(\vec{r})] + E_c^{GGA}[n(\vec{r})] \tag{2.48}$$

$$E_{xc}^{hybrid}[n(\vec{r})] = \frac{1}{4} E_x^{exact}[n(\vec{r})] + \frac{3}{4} E_x^{GGA}[n(\vec{r})] + E_c^{GGA}[n(\vec{r})] \tag{2.49}$$

2.5 Electronic Approximations

Pseudopotentials

The Kohn-Sham orbitals used to express the single particle density can be expanded into a basis set such as a plane wave basis set based on the Blöch theorem (as in Eq. 2.50 below) which is appropriate to in describe the electrons in a periodic potential observed in solids.[28] Aslo, as the kinetic energy operator is diagonal in a plane wave basis set and the potential in real space, we can utilize fast fourier transforms for switching between the representations which reduces the computational cost.[29]

$$\psi_{\vec{k}}^{n}(\vec{r}) = \sum_{\vec{K}} c_{\vec{K}}^{n,\vec{k}} e^{i(\vec{k}+\vec{K})\vec{r}} \tag{2.50}$$

However, the major disadvantage of a plane wave basis set is its inefficiency since, the number of basis sets required to describe atomic eigen functions close to nucleus would be enormous. This difficulty is addressed by the implementation of pseudopotentials representing the potential of ionic core and the core electrons since, the materials properties (physical or chemical) are governed largely by the valence electrons only. This is subject to certain criteria such as, (i) valence eigen functions should remain unchanged outside the core region r_c, (ii) pseudo eigen function within the core should match exactly at the boundary, (iii) pseudo eigen function and its first derivative should be continuous at the boundary and (iv) the pseudo eigen function is nodeless within the core region. These conditions are graphically presented in Fig. 2.1 where, the eigen function of a coulomb potential of the nucleus is presented in blue and the pseudo eigen function in red.[30] The real and pseudo eigen functions along with the potentials match beyond certain cut-off radius known as the core radius r_c.

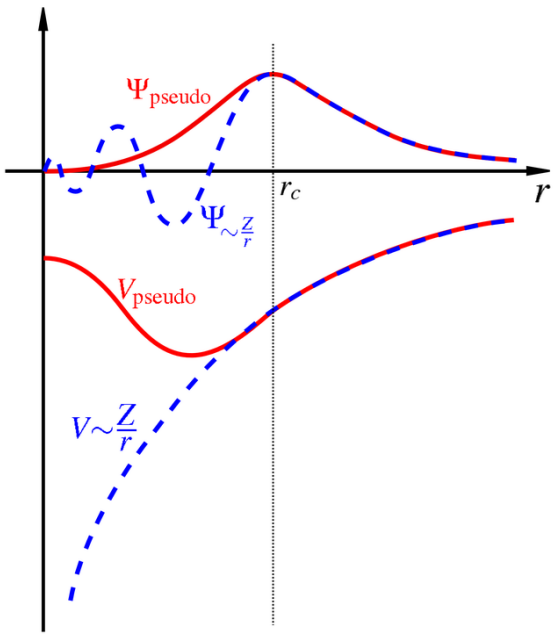

Figure 2.1: A schematic representation of pseudopotential. Adopted from *Phys. Rev. B.*, **50**, 17953-17979, (1994).

$$\psi = \tilde{\psi} + \sum_{i}^{n} c_i \phi_i - \sum_{i}^{n} c_i \tilde{\phi}_i \tag{2.51}$$

Pseudopotentials of diffreent classes have been developed over the years, for example, norm-conserving, ultra-soft, projector-augmented wave method etc.[31–33] Especially, the projector-augmented wave method is a significant improvement over the original techniques since it is an all-electron eigen function which consists of three parts as presented in Eq. 2.51 where, $\tilde{\psi}$ is the pseudo eigen function, ϕ_i is the all electron partial eigen function, $\tilde{\phi}_i$ is pseudo partial eigen function. Here, the pseudo eigen functions are represented by the plane waves which provide a good description of the eigen functions in regions far away from the ion core but deviates significantly from the all electron eigen functions near the ionic core. Thus, the all electron eigen functions in Eq. 2.51 are introduced to account for this error.

van der Waals Corrections

Under the standard framework of local density approximation or the generalised gradient approximation in density functional theory, the description of long-range dispersion forces are not accurately incorporated. This is necessary to compute the adsorption properties of molecules over surfaces and interfaces. To solve this issue, Grimme proposed a semi-empirical van der Waals correction method famously known as the D2 and D3 correction which accurately incorporate the long-range dispersion forces into the standard density functional theory.[34–36] The total energy of the Kohn-Sham system (E_{KS}) solved under the self-consistent field theory is corrected by incorporating the van der Waals correction term (E_{disp}) as presented in Eq. 2.52.

$$E_{DFT+D2/D3} = E_{KS} + E_{disp} \tag{2.52}$$

In the D2 scheme; a semi-empirical dispersion potential (C_6R^{-6}) and damping function (f_{damp}, at small atomic distances) are added to the Kohn-Sham energy in the form of a correction term presented in Eq. 2.53.

$$E_{disp} = -S_6 \sum_{i=1}^{N_{at}-1} \sum_{j=i+1}^{N_{at}} \frac{C_6^{ij}}{R_{ij}^6} f_{damp}(R_{ij}) \tag{2.53}$$

Whereas, in the D3 scheme, two-body ($E^{(2)}$) and three-body ($E^{(3)}$) energies sum-up forming the dispersion correction term E_{disp} which is incorporated into the Kohn-Sham energy wherein the terms ($E^{(2)}$) and ($E^{(3)}$) are presented in Eq. 2.54 and 2.55 respectively.

$$E^{(2)} = \sum_{AB} \sum_{\substack{n=2m \\ m=1,2,3,...}} S_n \frac{C_n^{AB}}{r_{AB}^n} f_{d,n}(r_{AB}) \tag{2.54}$$

$$E^{(3)} = \sum_{ABC} f_{d,(3)}(r_{ABC}) E^{(ABC)} \tag{2.55}$$

The global scaling factors S_n and S_6 in Eq. 2.53 and 2.54 depends explicitly on the exchange-correlation functional (i.e., for generalised gradient approximation functional such as PBE; $S_6 = 1.00$ and $S_8 = 0.72$). In equations above, C_6^{ij} and C_n^{AB} represent the n^{th} order dispersion coefficients for each '*ij*' and '*AB*' pair of atoms with interatomic distances R_{ij} and r_{AB} respectively. The damping functions (f_{damp} and $f_{d,n}$) are included to avoid singulatrities at small distances R_{ij} and r_{AB} with r_{ABC} as the average radii of a triple atom system '*ABC*' with $E^{(ABC)}$ representing a non-additive triple dipole dispersion term.

2.6 Lattice Dynamics, Elastic Constants and AIMD

Density Functional Perturbation Theory

To understand the structure, binding of atoms and ultimately the dynamical stability of a system, it is necessary to understand the vibrational energies and the displacement patterns which are known as the electronically excited states. Experimental this is achieved by performing IR and Raman spectroscopy. Hence, theoretically these phenomena can be addressed by the density functional perturbation theory wherein, the lattice dynamics of a material are investigated which governs, polarizability, phonons, IR and Raman spectra, superconductivity etc.[37–41] This is done by slightly perturbing the system from its ground state. Mathematically, this is achieved by taking the derivatives of the density functional theory electronic energies with respect to different perturbations.

$$V_{\lambda,ext}(\vec{r}) = V_{ext}(\vec{r}) + \lambda \frac{\partial V_{ext}(\vec{r})}{\partial \lambda} + \frac{1}{2}\lambda^2 \frac{\partial^2 V_{ext}(\vec{r})}{\partial \lambda^2} + ... \tag{2.56}$$

$$n_{\lambda}(\vec{r}) = n(\vec{r}) + \lambda \frac{\partial n(\vec{r})}{\partial \lambda} + \frac{1}{2}\lambda^2 \frac{\partial^2 n(\vec{r})}{\partial \lambda} + ... \tag{2.57}$$

$$E_\lambda(\vec{r}) = E(\vec{r}) + \lambda\frac{\partial E(\vec{r})}{\partial \lambda} + \frac{1}{2}\lambda^2\frac{\partial^2 E(\vec{r})}{\partial \lambda^2} + ... \tag{2.58}$$

In principle, we apply linear response theory to Kohn-Sham equations and observe the corresponding changes in the solution of electron densities under small perturbations. Therefore, V_{ext}, E, $n(\vec{r})$ etc. are subjected to perturbations in density functional perturbation theory. We can expand the external potential into a Taylor series in terms of some parameter γ as presented in Eq. 2.56. Similarly, we can expand the electron density $n(\vec{r})$ and the energy functional E as presented in Eq. 2.57 and 2.58 respectively.

In Eq. 2.58, $\frac{\partial E(\vec{r})}{\partial \lambda} = \int n(\vec{r})\frac{\partial V_{ext}(\vec{r})}{\partial \lambda}$ indicates that, the first order term in the expansion of the energy functional does not depend on the derivative of the electron density $n(\vec{r})$. However, the second order term has an explicit dependence on the first order derivative of the electron density. Hence, we proceed with the second order term of the energy functional expansion to compute the dynamical matrices for phonon frequencies and effective Born charges.[37–41] The energy functional in terms of the electron density is presented in Eq. 2.59. Then the second order term of the energy functional is obtained by variational principle (presented in Eq. 2.60) with respect to the first order eigen functions provided, the first order eigen functions are orthogonal to the ground state eigen functions (as presented in Eq. 2.61).

$$E[\psi] = \psi^{(1)}_{min}\sum_{i\in occ}\langle\psi_i|T + V_{ext}|\psi_i\rangle + E_{H,xc}[n] \tag{2.59}$$

$$\begin{aligned}\frac{\partial^2 E(\vec{r})}{\partial \lambda^2} = \psi^{(1)}_{min}\sum_{i\in occ}\Big[&\langle\psi_i^{(1)}|H^{(0)} - \epsilon_i^{(0)}|\psi^{(1)}\rangle + \langle\psi_i^{(1)}|V_{ext}^{(1)}|\psi_i^{(0)}\rangle + \langle\psi_i^{(0)}|V_{ext}^{(1)}|\psi_i^{(1)}\rangle + \\ &\langle\psi_i^{(0)}|V_{ext}^{(2)}|\psi_i^{(0)}\rangle\Big] + \frac{1}{2}\frac{\delta^2 E_{H,xc}}{\delta n(\vec{r})\delta n(\vec{r}')}\bigg|_{n^{(0)}} n^{(1)}(\vec{r})n^{(1)}(\vec{r}')d^3\vec{r}d^3\vec{r}' \\ &+ \int\left(\frac{d}{d\lambda}\frac{\delta E_{H,xc}}{\delta n(\vec{r})}\bigg|_{n^{(0)}} n^{(1)}(\vec{r})d^3\vec{r}\right)\frac{1}{2}\frac{d^2 E_{H,xc}}{d\lambda^2}\bigg|_{n^{(0)}}\end{aligned} \tag{2.60}$$

$$\langle\psi_i^{(0)}|\psi_j^{(j)}\rangle = 0 \tag{2.61}$$

The resulting dynamical matrices are Hermitian i.e., the constituent eigen values $\omega_j^2(\vec{q})$ and eigen vectors/functions $\xi_j(\vec{q})$ would be real and orthonormal respectively. In such scenarios, the phonon dispersions correspond to the phonon density of states which gives information about the entire brillouin zone.

The whole phonon dispersion spectra can be obtained by matrix diagonalization ($\mathcal{D}_{\alpha\beta}$) spanning over the three dimensional space of the wave vector $\vec{q}$ in the entire brillouin zone.[38–41] The resultant phonon density of states is determined by summation over every phonon state and is given as in Eq. 2.62 below where, $\mathcal{D}'$ is the normalization constant such that, $\int g(\omega)d\omega = 1$; with g($\omega$)d$\omega$ as a fraction of phonons with energies in the range ω to $\omega + d\omega$.[37–41]

$$g(\omega) = \mathcal{D}' \int_{BZ} \sum_{j} \delta(\omega - \omega_j(q))dq = \mathcal{D}' \int_{BZ} \sum_{j,p} \delta(\omega - \omega_j(q))dq_p \tag{2.62}$$

Here, the mesh indices 'p' are characterized by the wave vectors '$\vec{q}$' in the discrete irreducible brillouin zone where, dq_p gives the weight factor corresponding to the volume of the pth mesh in the $\vec{q}$ space.

Elastic Properties

Apart from the spectral properties (which can be computed under the density functional perturbation theory) the mechanical properties of materials are of great relevance since they give information regarding the nature of the material and its practical applicability. This is achieved by computing the elastic constants of materials which can be performed when the groud state structure in equilibrium configuration is known.

The system is perturbed from its equilibrium position by application of discrete strain fields and the corresponding atomic positions are relaxed. The numerical derivative of energy with respect to such strain gives the stress corresponding to the strained lattice. Therefore, stress as a function of strain is obtained, through which the elastic properties of a material can be determined by Birch-Murnaghan curve fitting.[42,43] The elastic constants corresponding to the second derivative of energy with respect to the strain tensor for a unit volume are presented in Eq. 2.63 where, ϵ_{kl} and σ_{ij} are the components of strain and stress tensors respectively.

$$C_{ijkl} = \frac{\sigma_{ij}}{\epsilon_{kl}} \tag{2.63}$$

The tensor C$_{ijkl}$ is a 6×6 matrix comprising of the independent elastic constants, C$_{ij}$ which is determined by the crystal symmetry. Therefore, the bulk, shear and, young's modulus can be calculated by applying different averaging approaches such as the one proposed by, Reuss, Voigt and Hill. Under the Voigt and Reuss averaging approach we can compute the bulk and shear modulus as presented in Eq. 2.64, 2.65 and 2.66, 2.67 respectively.

$$\mathcal{B}_V = \frac{1}{9}\left[(c_{11} + c_{22} + c_{33}) + 2(c_{12} + c_{23} + c_{13})\right] \tag{2.64}$$

$$\mathcal{G}_V = \frac{1}{15}\left[(c_{11} + c_{22} + c_{33}) - (c_{12} + c_{23} + c_{13}) + 3(c_{44} + c_{55} + c_{66})\right] \tag{2.65}$$

$$\mathcal{B}_R = \frac{1}{9}\left[(\sigma_{11} + \sigma_{22} + \sigma_{33}) + 2(\sigma_{12} + \sigma_{13} + \sigma_{23})\right] \tag{2.66}$$

$$\mathcal{G}_V = \frac{1}{15}\left[(\sigma_{11} + \sigma_{22} + \sigma_{33}) - (\sigma_{12} + \sigma_{13} + \sigma_{23}) + 3(\sigma_{44} + \sigma_{55} + \sigma_{66})\right] \tag{2.67}$$

Hill proposed that, Voigt and Reuss averaging aproaches serve as upper and lower limits of the elastic moduli respectively. Therefore, the Hill averaged approach gives bulk and shear modulus as presented in Eq. 2.68 and 2.69. Then using the bulk and shear moduli we can obtain other elastic moduli such as the yound's modulus $\mathcal{E}$ and the poisson ratio ρ as presented in Eq. 2.70 and 2.71 respectively.

$$\mathcal{B}_H = \frac{1}{2}(\mathcal{B}_V + \mathcal{B}_R) \tag{2.68}$$

$$\mathcal{G}_H = \frac{1}{2}(\mathcal{G}_V + \mathcal{G}_R) \tag{2.69}$$

$$\mathcal{E} = \frac{9\mathcal{B}_H\mathcal{G}_H}{3\mathcal{B}_H + \mathcal{G}_H} \tag{2.70}$$

$$\rho = \frac{3\mathcal{B}_H - 2\mathcal{G}_H}{2(3\mathcal{B}_H + \mathcal{G}_H)} \tag{2.71}$$

Apart from the mechanical properties which can be extracted from the equations above, we can also comment about the machanical stability of materials based on the Born-Huang criteria for the bulk and low dimensional materials which talk about the material stability in terms of the elastic tensors.[44] This is important because, a crystal system cannot exist in a stable or a meta-stable phase if their elastic tensors do not obey the Born-Huang stability criteria. For example, the stability criteria for a bulk cubic system are presented in Eq. 2.72 and for a low dimensional hexagonal system are presented in Eq. 2.73.[45,46]

$$c_{11} + 2c_{12} > 0; c_{44} > 0; c_{11} - c_{12} > 0 \tag{2.72}$$

$$c_{11} > 0; c_{11} - c_{12} > 0; c_{66} > 0 \tag{2.73}$$

ab-initio Molecular Dynamics

Classical molecular dynamics simulations deviate from the quantum mechanical approach, making it reliable for prediction of dynamics on meso-scopic scales. However, ab-initio molecular dynamics originates from a different approach and is used to get insights into the effects of temperature and the structural stability of materials. It exploits the fact that, atomic motions in periodic potentials obey Newtons second law of motion. So, rather than computing forces from classical mechanics, in ab-initio method, the forces are computed from ground state electron density obtained by the density functional theory. This makes ab-initio method highly accurate as compared to the coarsed approach of classical molecular dynamics, although, the disadvantage is associated computational cost. Hence, ab-initio method is just confined to a few hundred atoms. However, for for relatively simple systems, this method is quite feasible with proper balance in accuracy and computational time. In this thesis we employ, ab-initio molecular dynamics to estimate the structural properties of material at a particular temperature. This is achieved by a proper choice of thermostat out of, Gaussian, simple velocity rescaling, Berendsen, Bussi-Donadio-Parrinello, Andersen etc.[47–50]

In the Gaussian thermostat, the instantaneous temperature is exactly equal to the target temperature which is achieved by modifying the force as, $F = F_{interaction} + F_{constraint}$, where $F_{interaction}$ is the typical interactions force computed during simulation and $F_{constraint}$ is a Lagrangian multiplier such that, the kinetic energy is constant. Such a thermostat does not sample the canonical distribution rather it samples the isokinetic. Hence, the position-dependent (structural) properties can be obtained using this thermostat but not the velocity-dependent (dynamical) properties.[47]

The simple velocity rescaling thermostat is a non-physical thermostat although it is the easiest to implement. In this scheme, the particle momentum is rescaled in such a way that, the instanteneous temperature correlates to the target temperature similar to the Gaussian thermosat which leads to isokinetic ensemble. However, this scheme fails to properly sample the isokinetic ensemble so it is not recommended. Berendsen thermostat is a weak coupling thermostat the simple velocity rescaling thermostat. However, since it samples neither canonical nor the isokinetic distribution, it is not recommended.[47]

Bussi-Donadio-Parrinello thermostat is also known as, Canonical Sampling through Velocity Rescaling. In such a thermostat, the rescaling is done to kinetic energy which is stochastically selected from the kinetic energy distribution under the canonical ensemble scheme. Hence, this thermostat properly samples canonical ensemble and similar to the Berendsen thermostat, a time coupling parameter can be introduced to vary the velocity rescaling. This thermostat is reliable since the choice of time coupling constant does not affect structural properties and dynamical properties.[49]

Andersen thermostat selects particles randomly and facilitates a collision among them in a heat bath wherein the particle attains new velocity governed by the Maxwell-Botlzmann distribution. Such a thermostat can easily reproduce a canonical ensemble. Hence, it can be used to account for the structural properties of the material. We implement this thermostat in our ab-initio molecular dynamics to assertain the structural stability of low dimensional systems.[50]

2.7 Boltzmann Transport Theory

Transport properties of materials are governed by the response of carriers (such as, electrons or phonons) to external fields such as electric, magnetic or temperature gradient. Such carrier motion gives rise to finite electric or thermal conductivity owing to the exchange of energy and momentum due to scattering from crystal impurities under the influence of external fields.

Boltzmann transport theory deals with various transport parameters such as, the Seebeck coefficient, electrical conductivity, and electronic thermal conductivity.[51] These parameters are computed by solving the semi-classical Boltzmann transport equation which considers various external parameters effecting the transport properties of a material in the constant relaxation time approximation regime.[51] These equation have to be solved iteratively to compute the electron, phonon contributions to the thermoelectric properties. We begin with a distribution function *f(r,k,t)* which defines, the number of carriers in state '*k*' around a point '*r*' at time '*t*'. Such a distribution function can change over time by the virtue of, (i) diffusion, (ii) influence of external fields and, (iii) scattering/collisions. The evolution of such a system can be determined by computing the time derivative which leads to the semi-classical Boltzmann transport equation presented in Eq. 2.74 which reduces to Eq. 2.75 in case of a steady state system where, the net rate of change of distribution function *f(r,k,t)* is zero. These equations

are solved by following different approximations, off which the relaxation time approximation is the most reliable technique.

$$\frac{f(r,k,t)}{\partial t} = -v_k \frac{\partial f_k}{\partial r} - k\frac{\partial f(r,k,t)}{\partial k} - \frac{f(r,k,t) - f^0(r,k,t)}{\tau_k} \tag{2.74}$$

$$-v_k \frac{\partial f_k}{\partial r} - k\frac{\partial f(r,k,t)}{\partial k} - \frac{f(r,k,t) - f^0(r,k,t)}{\tau_k} = 0 \tag{2.75}$$

The energy conversion (from thermal to electrical and vice-versa) efficiency of a material is quantified by the figure of merit presented in Eq. 2.76 where, 'S' is Seebeck coefficient, 'σ' is the electrical conductivity, 'T' is temperature, 'κ_e' and 'κ_l' are the electronic and lattice contributions of thermal conductivity respectively. The electronic contribution to thermoelectrics is computed using the Boltzmann transport equations whereas the lattice constributions are computed using the phonon Boltzmann transport equation wherein the third order phonon scattering effects are incorporated. This is implemented in the ShengBTE code.

$$zT = \Big(\frac{S^2\sigma}{\kappa_e + \kappa_l}\Big)T \tag{2.76}$$

The electronic contributions to thermoelectric transport properties are computed by extrapolating the electronic band dispersion energies under Fourier expansion. This is done under the constant relaxation time approximation wherein the Seebeck coefficient of the system is independent of the scattering rates.[52] However, one issue is that, the electrical conductivity (σ) and the electronic thermal condcutivity (κ_e) are computed as a function of the relaxation time (τ). Similarly, the lattice contribution to thermal conductivity (κ_l) is computed in terms of the third order interatomic force constants since, the second order interatomic force constants under harmonic approximation neglect the crystal anharmonicity. Further, the deformation potential theory is implemented to compute transport parameters independent of the relaxation time as proposed by Bardeen and Shokley, wherein the carrier mobility (μ) can be used to estimate the relaxation time (τ) as presented in Eq. 2.77 and 2.78 respectively, where, C_{ii} are the elastic constants and E_1 is the deformation potential constant.[53] The later is computed by subjecting the system to strain of the form $\pm\delta(x)$ and the corresponding valence band maxima ($E^{(VBM)}$) and conduction band minima ($E^{(CBM)}$) energies are computed from the electronic dispersion relation to incorporate the hole and electron dependent properties respectively.[53] However, these band energies are corrected and realigned with respect to the core energy ($E^{(core)}$) at the corresponding strain. The plot of these aligned eigen values with

strain is linear in nature wherein, on linear fit; the slope represents the deformation potential constant.

$$\mu = \frac{(8\pi)^{1/2}\hbar^4 e C_{ii}}{(m^*)^{5/2}(k_B T)^{3/2} E_1^2} \tag{2.77}$$

$$\tau = \frac{\mu m^*}{e} \tag{2.78}$$

Thermally activated electrons and holes are vital in transport phenomena of inorganic materials since they exhibit highly coherent wavelengths longer than the lattice constant with the magnitudes close to the acoustic phonon mode at the center of brillouin zone.[54] The dimensional quantum confinement is known to alter the transport properties and the associated dynamics such as, electron-phonon coupling and scattering mechanisms. Hence, it is necessary to incorporate these scenarios by extending the deformation potential theory to low dimensional materials which was proposed by Bardeen and Shockley.[52,55,56] It was eventually shown that, the carrier mobilities explicitly demonstrate the effects of dimensional quantum confinement.[57–59]

2.8 Topological Properties

The topological properties in terms of, $\mathbb{Z}_2$ invariant, slab-band structures, angle resolved photoemission spectroscopy etc. lie at the core of investigations performed in this thesis. These properties can be obtained by transforming the plane wave basis set in the reciprocal space to maximally localised wannier functions in real space. This helps generate the tigh-binding model which is used to obtain the the required properties. Here we discuss various methods which are developed to compute the said topological properties, beginning from the theory of maximally localised wannier functions, *Berry* connection and the *Berry* curvature, spin Hall conductivity, the tight-binding Hamiltonian model, wannier charge centers, methods to compute $\mathbb{Z}_2$ invariants etc.

Maximally Localised Wannier Functions

The maximally localised wannier functions approach was developed by Marzari and Vanderbilt to transform the eigen functions from spanning the reciprocal space to be localised in real space.[60,61] In a typical *first-principles* calculation, the electronic structure of periodic systems

defined by the extended Blöch states for nth band with crystal momentum 'k' as ψ_{nk}. However, Marzari and Vanderbilt gave an alternate approach wherein, the spatially localised wannier functions centred at a crystal lattice site R, $\omega_n R(\vec{r})$ are represented in terms of the Blöch states as presented in Eq. 2.79 where, V is the unit cell volume, $U^{(k)}$ is a unitary matrix to mix the Blöch states at each crystal momentum 'k'. Since, the unitary matrix $U^{(k)}$ is not uniquely defined, different choice of such matrix would lead to different spacial localisation of the wannier functions.

$$\omega_n R(\vec{r}) = \frac{V}{(2\pi)^3} \int_{BZ} \Big[\sum_m U_{mn}^{(k)} \psi_{mk}(\vec{r}) \Big] e^{-k.R} dk \tag{2.79}$$

The speard (Ω) of a wannier function is presented in Eq. 2.80 such that, it can be decoupled into a gauge invariant term (Ω_I) and a term ($\tilde{\Omega}$) which depends on the gauge choice of $U^{(k)}$. The latter can be further decomposed into diagonal (Ω_D) and off-diagonal (Ω_{OD}) terms constituting the wannier functions as presented in Eq. 2.81.

$$\Omega = \sum_n \left[\langle \omega_{n0}(\vec{r}) | \vec{r}^2 | \omega_{n0}(\vec{r}) \rangle - | \langle \omega_{n0}(\vec{r}) | \vec{r} | \omega_{n0}(\vec{r}) \rangle |^2 \right] \tag{2.80}$$

$$\Omega = \Omega_I + \tilde{\Omega} = \Omega_I + \Omega_D + \Omega_{OD} \tag{2.81}$$

Where,

$$\Omega_I = \sum_n \left[\langle \omega_{n0}(\vec{r}) | \vec{r}^2 | \omega_{n0}(\vec{r}) \rangle - \sum_{Rm} | \langle \omega_{nR}(\vec{r}) | \vec{r} | \omega_{n0}(\vec{r}) \rangle |^2 \right] \tag{2.82}$$

$$\Omega_D = \sum_n \sum_{R \neq 0} | \langle \omega_{nR}(\vec{r}) | \vec{r} | \omega_{n0}(\vec{r}) \rangle |^2 \tag{2.83}$$

$$\Omega_O D = \sum_{m \neq n} \sum_R | \langle \omega_{nR}(\vec{r}) | \vec{r} | \omega_{n0}(\vec{r}) \rangle |^2 \tag{2.84}$$

In order to obtain, the maximally localised wannier functions, Marzari and Vanderbilt proposed to minimize the gauge dependent spread function ($\tilde{\Omega}$) with respect to a set of unitary matrices $U^{(k)}$.[60] For this purpose, two key ingredients are obtained from the first-principles electronic structure calculations i.e., (i) the overlap between cell periodic part of Blöch states ($|u_{nk}\rangle$) are computed over vectors which connects a given k-point to its neighbours as presented in Eq. 2.85 and, (ii) initially by guess, the Blöch states ($|\psi_{nk}\rangle$) are projected onto a localised

orbital ($|g_n\rangle$) (as presented in Eq. 2.86) such that, the small N × N matrices $M^{(k,b)}$, $A^{(k)}$ and $U^{(k)}$ are independent of the basis set used to obtain the original Blöch states.[60]

$$M_{mn}^{(k,b)} = \langle u_{mk} | u_{nk+b} \rangle \tag{2.85}$$

$$A_{mn}^{(k)} = \langle \psi_{mk} | g_n \rangle \tag{2.86}$$

Berry Connection and Curvature

In terms of periodic Blöch states ($|u_{nk}\rangle = e^{-ik.r}|\psi_{nk}\rangle$), the Berry connection is defined as in Eq. 2.87. Then, the curl of Berry connections gives the Berry curvature as presented in Eq. 2.88.

$$A_n(k) = \langle u_{nk} | i\nabla_k | u_{nk} \rangle \tag{2.87}$$

$$\Omega_n(k) = \nabla_k \times A_n(k) = -\mathrm{Im} \langle \nabla_k u_{nk} | \times | \nabla_k u_{nk} \rangle \tag{2.88}$$

The quantities presented in Eq. 2.87 and 2.88 are central to the description of electronic properties of crystals.[62]

Spin Hall Conductivity

Under the independent particle approximation, the spin Hall conductivity of a material is given by the Kubo-Greenwood formula presented in Eq. 2.89.

$$\sigma_{\alpha\beta}^{\mathrm{spin}\,\gamma}(\omega) = \frac{\hbar}{\Omega_c N_k} \sum_k \sum_n f_{nk} \sum_{m \neq n} \frac{2\,\mathrm{Im}\left[\langle nk | \hat{j}_\alpha^\gamma | mk \rangle \langle mk | - e\hat{v}_\beta | nk \rangle\right]}{(\epsilon_{nk} - \epsilon_{mk})^2 - (\hbar\omega + i\eta)^2} \tag{2.89}$$

Here, $\hat{j}_\alpha^\gamma = \frac{1}{2}\{\hat{s}_\gamma, \hat{v}_\alpha\}$ is the spin current operator with the spin operator $\hat{s}_\gamma = \frac{\hbar}{2}\hat{\sigma}_\gamma$ where, α and β represent the cartesian directions and γ represents the spin direction which are typically x, y and z respectively. Ω_c is the cell volume, N_k are the number of k-points used to sample the brillouin zone, f_{nk} is the Fermi-Dirac distribution function, $\hbar\omega$ is the optical frequency and η is a smearing paramter in energy units.

The velocity matrix in the numerator of Eq. 2.89 is a known quantity, however, the spin current matrix $\langle nk | \hat{j}_\alpha^\gamma | mk \rangle$ which is unknown term can be computed using wannier

interpolation method. Eq. 2.89 can be further resolved into a band projected Berry curvature like term presented in Eq. 2.90 such that, the momentum resolved term summing over the occupied bands is presented in Eq. 2.91. Then the final form of the spin Hall conductivity is presented in Eq. 2.92.[64]

$$\Omega^{\text{spin}\,\gamma}_{n,\alpha\beta}(k) = \hbar^2 \sum_{m\neq n} \frac{-2\,\text{Im}\left[\langle nk|\frac{1}{2}\{\hat{s}_\gamma, \hat{v}_\alpha\}|mk\rangle\langle mk| - e\hat{v}_\beta|nk\rangle\right]}{(\epsilon_{nk} - \epsilon_{mk})^2 - (\hbar\omega + i\eta)^2} \tag{2.90}$$

$$\Omega^{\text{spin}\,\gamma}_{\alpha\beta}(k) = \sum_n f_{nk}\Omega^{\text{spin}\,\gamma}_{n,\alpha\beta}(k) \tag{2.91}$$

$$\sigma^{\text{spin}\,\gamma}_{\alpha\beta}(\omega) = -\frac{e^2}{\hbar}\frac{1}{\Omega_c N_k}\sum_k \Omega^{\text{spin}\,\gamma}_{\alpha\beta}(k) \tag{2.92}$$

Where the unit of $\Omega^{\text{spin}\,\gamma}_{\alpha\beta}(k)$ is Å^2 and the unit of $\sigma^{\text{spin}\,\gamma}_{\alpha\beta}(\omega)$ is $(\hbar/e)Scm^{-1}$ wherein, for $\omega = 0$ we have the DC spin Hall conductivity and for $\omega \neq 0$ we have the frequency dependent or AC spin Hall conductivity. Eq. 2.91 is used to compute momentum resolved, band projected spin Berry curvature.

Tight-Binding Model

A semi-empirical approach to study electronic structures of periodic systems by projecting the Hamiltonian onto a series of localised orbitals is known as the tight-binding method. There are three methods to generate and construct such as model which are, (i) Slater-Koster method, (ii) discrete k·p model on a lattice and (iii) maximally localised wannier functions.[65–67] Over the years, the maximally localised wannier functions have gained a lot of popularity to generate tight-binding model for predicting materials properties. The basis functions in a tight-binding method can be mutually orthogonal or non-orthogonal. Wannier functions generate orthogoal basis functions for the tight-binding model which is implemented in WannierTools code to predict material properties.[67]

To generate the tight binding model, consider, 'i' atoms with 'μ' orbitals such that, the combination is labelled as, $\{i,\mu\}$ with, '$\vec{R}$' representing the lattice vactors of the three dimensional periodic arrangement and τ_i indicating the position of atoms in the unit cell. Then, the local orbital of i^{th} atom centered at $(\vec{R} + \vec{\tau}_i)$ can be presented as in Eq. 2.93.

$$\phi_{Rm}(\vec{r}) \equiv \phi_m(\vec{r} - \vec{R}) \equiv \varphi_{i\mu}(\vec{r} - \vec{R} - \vec{\tau}_i) \tag{2.93}$$

Since the basis functions have to be orthogonal, the need to satisfy the relation, $\langle \phi_{Rm} | \phi_{R'm} = \delta_{RR'}\delta_{mn}$. Then, the tight-binding parameters of the Hamiltonian with translational symmetry under the Blöch periodic codition is given as presented in Eq. 2.94.

$$H_{mn}(\vec{R}) = \langle \phi_{0m} | \hat{H} | \phi_{Rn} \tag{2.94}$$

Using the tigh-binding Hamiltonian presented in Eq. 2.94, we can present the tigh-binding Hamiltonian in momentum space by performing a Fourier transformation under two conventions presented in Eq. 2.95 and 2.96.[67]

$$H_{mn}(k) = \sum_{R} e^{ik\cdot R} H_{mn}(\vec{R}) \tag{2.95}$$

$$H_{mn}(k) = \sum_{R} e^{ik\cdot(R+\tau_m-\tau_n)} H_{mn}(\vec{R}) \tag{2.96}$$

The eigen values obtained under the two conventions prsented in Eq. 2.95 and 2.96 are identical but the eigen functions are different i.e., eigen functions in Eq. 2.95 are similar to the Blöch eigen functions $\psi_{nk}(\vec{r})$ and, the eigen functions in Eq. 2.96 are similar to the periodic Blöch eigen functions $u_{nk}(\vec{r}) = \psi_{nk}(\vec{r})e^{-ikr}$. We use the tight-binding Hamiltonian presented in Eq. 2.96 to compute material properties.

Topological Invariants

The topological insulators are classified into trivial and non-trivial characters by computing the $\mathbb{Z}_2$ invariants and the Chern numbers.[68,69] The former is used in case of systems where the time-reversal is invariant and the later is used in case of systems where the time-reversal symmetry is broken. We will proceed with discussions of the $\mathbb{Z}_2$ invariants.

Fu and Kane proposed that, for systems governed by the inversion symmetry in bulk and low dimensional phase, the $\mathbb{Z}_2$ invariants can be computed by taking the product of parities of the Kramer degenerate occupied eigen states at time reversal invariant momenta and parity invariant points in the brillouin zone.[70]

Equation 2.97 and 2.98 are used to compute the $\mathbb{Z}_2$ invariants for bulk materials since, the bulk has eight time-reversal invariant points which leads to four independent $\mathbb{Z}_2$ invariants. One of them is ν_0, which is computed as the product over all the eight points (as presented in

Eq. 2.97) and the other three (ν_1, ν_2, ν_3) are computed as products over four δ_i for which the time reversal invariant momenta lie in the same plane.[70]

$$(-1)^{\nu_0} = \prod_{i=1}^{8} \delta_i \tag{2.97}$$

$$(-1)^{\nu_k} = \prod_{\substack{n_k=1; \\ n_{j\neq k}=0,1}} \delta_{i=(n_1 n_2 n_3)} \tag{2.98}$$

Equation 2.99 presents the $\mathbb{Z}_2$ for low dimensional materials wherein, the product of parities are computed only along four time-reversal invariant momenta.[70]

$$(-1)^{\nu} = \prod_{i=1}^{4} \delta_i \tag{2.99}$$

However, for systems violating the time-reversal symmetry, the method of computing $\mathbb{Z}_2$ invariat is based on the wilson loop and wannier charge center methods.[71,72] It was found that, both of these methods accurately predict the $\mathbb{Z}_2$ invariants in systems violating the time-reversal symmetry. For systems obeying time-reversal symmtry, the $\mathbb{Z}_2$ could be computed in terms of the time-reversal polarization ($\mathcal{P}_\theta$) which is gauge invariant (as presented in Eq. 2.100).[70]

$$\Delta = \left[\mathcal{P}_\theta(\mathcal{T}/2) - \mathcal{P}_\theta(0)\right] mod 2 \tag{2.100}$$

This equation is modified into Eq. 2.101 and 2.102 wherein, the time-reversal polarization relation is modified in terms of the wannier charge centers along two momentum planes in the brillouin zone (as in Eq. 2.101 and 2.102).[72]

$$\nu_0 = \left[(\mathbb{Z}_2)_{k_i=0} + (\mathbb{Z}_2)_{k_i=0.5}\right] mod 2 \tag{2.101}$$

$$\nu_i = (\mathbb{Z}_2)_{k_i=0.5}, i = 1, 2, 3 \tag{2.102}$$

Surface States

It is a computationally expensive task to compute the slab band structures to observe the surface/edge states in topological systems. For this purpose, we employ, the tight-binding Hamiltonian model generated using wannier functions to compute the surface/edge states

using the surface Green's function for a semi-infinite system. The Green's function approach based on the effective field theory and transfer matrix converge slowly near singularities.[73–75] As an alternative, the iterative Green's function method developed in 1980's is used for faster convergence.[76,77] The faster convergence and resulting lower computational time is due to the principle layers (which are large enough to ensure that, the hoppings to next nearest layers are negligible). This is achieved by replacing the principle layers with an effective two principle layers such that, the interaction of effective layers is governed by the energy dependent residual interacctions which are weaker. This process of replaceing the layers is repeated iteratively until the interactions between the layers is quite small as per requirements.[78]

$$\mathcal{G}_s(k_{||}, \omega) \approx (\omega - \epsilon_n^s)^{-1} \tag{2.103}$$

$$\tilde{\mathcal{G}}_s(k_{||}, \omega) \approx (\omega - \tilde{\epsilon}_n^s)^{-1} \tag{2.104}$$

$$\mathcal{G}_b(k_{||}, \omega) \approx (\omega - \epsilon_n)^{-1} \tag{2.105}$$

The surface ($\mathcal{G}_s(k_{||}, \omega)$) and bulk ($\mathcal{G}_b(k_{||}, \omega)$) Green's function obtained from such iterative process are presented in Eq. 2.103 and 2.105 respectively where, $\tilde{\mathcal{G}}_s$ is the surface Green's function of a dual surface. Then, the surface/edge spectrum can be obtained from the imaginary part of the surface Green's function as presented in Eq. 2.106.

$$\mathcal{A}(k_{||}, \omega) = -\frac{1}{\pi} \lim_{\eta \to 0^+} \mathrm{Im}\,\mathrm{Tr}\,\mathcal{G}_s(k_{||}, \omega + i\eta) \tag{2.106}$$

2.9 Computational Packages

We use Quantum ESPRESSO open-source package which an integrated suite to perform; electronic-structure calculations and materials modeling at on bulk as well as nano-scale.[79] It is based on density functional theory, plane waves approximation and pseudopotential methods. Using this package, we performed *first-principles* computations under self-consistent field formalism to obtain the ground state eigen energies of the bulk and low dimensional periodic systems. For electronic structure calculations (wherein we compute the electronic eigen states as a function of crystal momentum) we perform computations in terms of non-self consistent field formalisms. This code is so versatile that, we can perform structural relaxations and

optimizations, compute the electronic charge densities, perform computations using van der Waals dispersion corrections, compute electronic-structure under the influence of spin-orbit interactions, compute the density of states and orbital projected density of states, compute vibrational properties under density functional perturbation theory etc. Another advantage of Quantum ESPRESSO code is that, due to its open-source availibility, it can be interfaced with several computational codes to compute other material properties. Several members of active computational physics group develop codes which can be easily interfaced with Quantum ESPRESSO increasing its capabilities.

Figure 2.2: Computational codes used in this thesis.

For example, using the ground state energies and the corresponsing crystal structure, we can interface the Quantum ESPRESSO code with the ElaStic code (a part of the Exciting code) to compute the elastic stress tensors.[80] This is achieved in ElaStic code by, perturbing the ground state system with small strain of the order of $\pm$ 5% or 10% (as per our requirement). The corresponding crystal structures are fed into Quantum ESPRESSO code and the respective ground state energies are computed. Then, the ElaStic code plots a curve of energy versus strain and performs linear or polynomial fitting eventually giving the elastic stress tensors.

For computing the thermoelectric transport properties, we employ the open-source BoltzTrap code which implements the semi-classical Botlzmann transport equations to compute the semi-classical transport coefficients.[81] This code is interfaced with Quantum ESPRESSO and uses a mesh of electronic-structures for computing the thermoelectric properties. Hence, we can get the insights into the electronic aspect of thermoelectric properties using this code. As far as the lattice or vibrational aspect is concerned, we use ShengBTE code which computes the semi-classical Boltzmann transport equations for phonons.[82] The 2^{nd} and 3^{rd} order inter-atomic force constants required in ShengBTE are obtained using Quantum ESPRESSO.

The topological properties are computed by employing open-source packages such as, Wannier90 and WannierTools code.[83,84] The Wannier90 code is used to generate the maximally localised wannier functions. These functions are obtained by performing fourier transforms of the plane wave basis set generated in Quantum ESPRESSO. The general workflow is that, we perform self-consisten field calculations on a system, then the non-consistent field calculations (which gives information about the distribution of eigen states in the momentum space), this is followed by the interfacing script *pw2wannier* (which performs the transformation of basis sets and generates the input parameters required for wannierisation) bridging Quantum ESPRESSO and Wannier90, then finally, wannierisation is performed to compute the maximally localised wannier functions. Using the maximally localised wannier functions obtained from Wannier90, we generate the exact tight-binding Hamiltonian model which would be interfaced with the WannierTools code.

We employed the maximally localised wannier functions to compute and investigate topological properties using WannierTools code. This code extracts the information from the exact tight-binding Hamiltonian generated using Wannier90 and computes topological properties such as, angle resolved photo-emission spectroscopy-like spectra, spin-textures, topological invariants (using Wilson loop method), slab band structures etc.

During the entire process of investigations and prediction of material properties, open-source packages such as, xcrysden and VESTA were extensively used.[85,86] These are crystalline and molecular structure visualisation programs used to, display and visualize the crystal structures and morphologies, trace the brillouin zone momentum path (for computing band structures and phonon dispersion curves), generate 2D and 3D plots of charge density profiles / contours using volumetric data of electronic and nuclear densities etc.

Bibliography

[1] Erwin Schrödinger.Physical review, 28(6):1049, 1926.

[2] John C. Slater.American Journal of Physics, 32(1):65–66, 1964.

[3] David S Sholl and Janice A Steckel.Density functional theory: a practical introduction. John Wiley & Sons, 2011.

[4] Robert Eisberg, Robert & Resnick.Quantum Physics of Atoms, Molecules, Solids, Nuclei, and Particles. John Wiley & Sons, 1985.

[5] Max Born and Robert Oppenheimer.Annalen der physik, 389(20):457–484, 1927.

[6] Charles A Coulson.Reviews of Modern Physics, 32(2):170, 1960.

[7] Douglas R Hartree. InMathematical Proceedings of the Cambridge Philosophical Society, volume 24, pages 89–110. Cambridge university press, 1928.

[8] Douglas Rayne Hartree. InMathematical Proceedings of the Cambridge Philosophical Society, volume 24, pages 111–132. Cambridge University Press, 1928.

[9] D R Hartree. InMathematical Proceedings of the Cambridge Philosophical Society, volume 24, pages 426–437. Cambridge University Press, 1928.

[10] D R Hartree. InMathematical Proceedings of the Cambridge Philosophical Society, volume 25, pages 310–314. Cambridge University Press, 1929.

[11] Douglas Rayner Hartree and William Hartree.Proceedings of the Royal Society of London. Series A-Mathematical and Physical Sciences, 150(869):9–33, 1935.

[12] John Clarke Slater.Physical Review, 32(3):339, 1928.

[13] John C Slater.Physical Review, 35(2):210, 1930.

[14] Vladimir Fock.Zeitschrift fur Physik, 61(1):126–148, 1930.

[15] John C Slater.Physical Review, 36(1):57, 1930.

[16] Llewellyn H Thomas. In Mathematical proceedings of the Cambridge philosophical society, volume 23, pages 542–548. Cambridge University Press, 1927.

[17] Enrico Fermi.Rend. Accad. Naz. Lincei, 6(602-607):5, 1927.

[18] Laurence D Hoffmann, Gerald L Bradley, and Kenneth H Rosen.Calculus for business, economics, and the social and life sciences. McGraw-Hill, 1989.

[19] Paul Adrien Maurice Dirac.Proceedings of the Royal Society of London. Series A, Containing Papers of a Mathematical and Physical Character, 133(821):60–72, 1931.

[20] CF von Weizsacker.Zeitschrift fur Physik, 96(7):431–458, 1935.

[21] Pierre Hohenberg and Walter Kohn.Physical review, 136(3B):B864, 1964.

[22] Walter Kohn and Lu Jeu Sham.Physical review, 140(4A):A1133, 1965.

[23] John P Perdew.Physical Review Letters, 55(16):1665, 1985.

[24] John P Perdew, Kieron Burke, and Matthias Ernzerhof.Physical review letters, 77(18):3865, 1996.

[25] Swapan K Ghosh and Robert G Parr.Physical Review A, 34(2):785, 1986.

[26] Axel D Becke and Marc R Roussel.Physical Review A, 39(8):3761, 1989.

[27] Axel D Becke.The Journal of chemical physics, 98(2):1372–1377, 1993.

[28] Felix Bloch.Zeitschrift fur physik, 52(7):555–600, 1929.

[29] Michael Heideman, Don Johnson, and Charles Burrus.IEEE ASSP Magazine, 1(4):14–21, 1984.

[30] Mike C Payne, Michael P Teter, Douglas C Allan, TA Arias, and ad JD Joannopoulos, Reviews of modern physics, 64(4):1045, 1992.

[31] D R Hamann, M Schluter, and C Chiang.Physical Review Letters, 43(20):1494, 1979.

[32] David Vanderbilt.Physical review B, 41(11):7892, 1990.

[33] Georg Kresse and Daniel Joubert.Physical review b, 59(3):1758, 1999.

[34] Stefan Grimme.Journal of computational chemistry, 27(15):1787–1799, 2006.

[35] Stefan Grimme.Journal of computational chemistry, 25(12):1463–1473, 2004.

[36] Stefan Grimme, Jens Antony, Stephan Ehrlich, and Helge Krieg.The Journal of chemical physics, 132(15):154104, 2010.

[37] Xavier Gonze.Physical Review A, 52(2):1096, 1995.

[38] Stefano Baroni, Stefano De Gironcoli, Andrea Dal Corso, and Paolo Giannozzi.Reviews of modern Physics, 73(2):515, 2001.

[39] Arnold M Kosevich.The crystal lattice: phonons, solitons, dislocations, superlattices. 2006.

[40] Ganesan Venkataraman, Lee A Feldkamp, and Vinod C Sahni.Dynamics of perfect crystals. 1975.

[41] S Yu Savrasov, D Yu Savrasov, and OK Andersen.Physical review letters, 72(3):372, 1994.

[42] Francis Birch.Physical review, 71(11):809, 1947.

[43] Francis Birch.Journal of Applied Physics, 9(4):279–288, 1938.

[44] Max Born and Kun Huang.Dynamical theory of crystal lattices. Oxford University Press, 1954.

[45] Jinghan Wang, Sidney Yip, SR Phillpot, and Dieter Wolf.Physical review letters, 71(25):4182, 1993.

[46] Guilherme SL Fabris, Carlos A Paskocimas, Julio R Sambrano, and Ricardo Paupitz, Journal of Solid State Chemistry, 303:122513, 2021.

[47] Philippe H Hunenberger.Advanced computer simulation, pages 105–149, 2005.

[48] Herman JC Berendsen, JPM van Postma, Wilfred F Van Gunsteren, ARHJ DiNola, and Jan R Haak.The Journal of chemical physics, 81(8):3684–3690, 1984.

[49] Giovanni Bussi, Davide Donadio, and Michele Parrinello.The Journal of chemical physics, 126(1):014101, 2007.

[50] Hans C Andersen.The Journal of chemical physics, 72(4):2384–2393, 1980.

[51] John M Ziman.Electrons and phonons: the theory of transport phenomena in solids. Oxford university press, 2001.

[52] J Bardeen and W Shockley.Physical review, 80(1):72, 1950.

[53] Yongqing Cai, Gang Zhang, and Yong-Wei Zhang.Journal of the American Chemical Society, 136(17):6269–6275, 2014.

[54] Kristen Kaasbjerg, Kristian S Thygesen, and Karsten W Jacobsen.Physical Review B, 85(11):115317, 2012.

[55] Kristen Kaasbjerg, Kristian S Thygesen, and Antti-Pekka Jauho.Physical Review B, 87(23):235312, 2013.

[56] Jinying Wang, Ruiqi Zhao, Mingmei Yang, Zhongfan Liu, and Zhirong Liu.The Journal of chemical physics, 138(8):084701, 2013.

[57] Jinyang Xi, Mengqiu Long, Ling Tang, Dong Wang, and Zhigang Shuai.Nanoscale, 4(15):4348–4369, 2012.

[58] Mengqiu Long, Ling Tang, Dong Wang, Yuliang Li, and Zhigang Shuai.ACS nano, 5(4):2593–2600, 2011.

[59] Meng-Qiu Long, Ling Tang, Dong Wang, Linjun Wang, and Zhigang Shuai.Journal of the American Chemical Society, 131(49):17728–17729, 2009.

[60] Nicola Marzari and David Vanderbilt.Physical review B, 56(20):12847, 1997.

[61] Ivo Souza, Nicola Marzari, and David Vanderbilt.Physical Review B, 65(3):035109, 2001.

[62] Di Xiao, Ming-Che Chang, and Qian Niu.Reviews of modern physics, 82(3):1959, 2010.

[63] Qiao, Junfeng and Zhou, Jiaqi and Yuan, Zhe and Zhao, Weisheng, Physical Review B, 98(21), 214402, 2018.

[64] Guang-Yu Guo, Shuichi Murakami, T-W Chen, and Naoto Nagaosa.Physical review letters, 100(9):096401, 2008.

[65] John C Slater and George F Koster.Physical Review, 94(6):1498, 1954.

[66] Lok C. Lew Yan Voon Morten Willatzen.The k p Method. Springer Berlin, Heidelberg, 2009.

[67] Nicola Marzari, Arash A Mostofi, Jonathan R Yates, Ivo Souza, and David Vanderbilt, Reviews of Modern Physics, 84(4):1419, 2012.

[68] Charles L Kane and Eugene J Mele.Physical review letters, 95(14):146802, 2005.

[69] D. J. Thouless, M. Kohmoto, M. P. Nightingale, and M. den Nijs.Phys. Rev. Lett., 49:405–408, Aug 1982.

[70] Liang Fu and C. L. Kane.Phys. Rev. B, 76:045302, Jul 2007.

[71] Rui Yu, Xiao Liang Qi, Andrei Bernevig, Zhong Fang, and Xi Dai.Phys. Rev. B, 84:075119, Aug 2011.

[72] Alexey A. Soluyanov and David Vanderbilt.Phys. Rev. B, 83:235401, Jun 2011.

[73] L M Falicov and F Yndurain.Journal of Physics C: Solid State Physics, 8(2):147–157, jan 1975.

[74] D. H. Lee and J. D. Joannopoulos.Phys. Rev. B, 23:4988–4996, May 1981.

[75] D. H. Lee and J. D. Joannopoulos.Phys. Rev. B, 23:4997–5004, May 1981.

[76] F. Guinea, C. Tejedor, F. Flores, and E. Louis.Phys. Rev. B, 28:4397–4402, Oct 1983.

[77] M P Lopez Sancho, J M Lopez Sancho, and J Rubio.Journal of Physics F: Metal Physics, 14(5):1205–1215, may 1984.

[78] M P Lopez Sancho, J M Lopez Sancho, J M L Sancho, and J Rubio.Journal of Physics F: Metal Physics, 15(4):851–858, apr 1985.

[79] P Giannozzi, O Andreussi, T Brumme, O Bunau, M Buongiorno Nardelli, M Calandra, R Car, C Cavazzoni, D Ceresoli, M Cococcioni, N Colonna, I Carnimeo, A Dal Corso, S de Gironcoli, P Delugas, R A DiStasio, A Ferretti, A Floris, G Fratesi, G Fugallo, R

Gebauer, U Gerstmann, F Giustino, T Gorni, J Jia, M Kawamura, H-Y Ko, A Kokalj, E Kuccukbenli, M Lazzeri, M Marsili, N Marzari, F Mauri, N L Nguyen, H-V Nguyen, A Otero de-la Roza, L Paulatto, and S Ponce. 29(46):465901, oct 2017.

[80] Rostam Golesorkhtabar, Pasquale Pavone, Jürgen Spitaler, Peter Puschnig, and Claudia Draxl.Computer Physics Communications, 184(8):1861–1873, 2013.

[81] Georg K.H. Madsen and David J. Singh.Computer Physics Communications, 175(1):67–71, 2006.

[82] Wu Li, Jesús Carrete, Nebil A. Katcho, and Natalio Mingo.Computer Physics Communications, 185(6):1747–1758, 2014.

[83] Arash A. Mostofi, Jonathan R. Yates, Giovanni Pizzi, Young-Su Lee, Ivo Souza, David Vanderbilt, and Nicola Marzari.Computer Physics Communications, 185(8):2309– 2310, 2014.

[84] QuanSheng Wu, ShengNan Zhang, Hai-Feng Song, Matthias Troyer, and Alexey A. Soluyanov.Computer Physics Communications, 224:405–416, 2018.

[85] Anton Kokalj.Journal of Molecular Graphics and Modelling, 17(3):176–179, 1999.

[86] Koichi Momma and Fujio Izumi.Journal of Applied Crystallography, 41(3):653–658, Jun 2008.